Hindawi
Geofluids
Volume 2022, Article ID 7001654, 11 pages
https://doi.org/10.1155/2022/7001654

Research Article

Analysis of the Coal Fluidization Mining Process with the Continuous-Discontinuous Coupled Particle-Block Method

Jing Li,[1] Chun Feng,[2] Xinguang Zhu,[2] and Yiming Zhang[1]

[1]*School of Civil and Transportation Engineering, Hebei University of Technology, Xiping Road 5340, 300401 Tianjin, China*
[2]*Key Laboratory for Mechanics in Fluid Solid Coupling Systems, Institute of Mechanics, Chinese Academy of Sciences, Beijing, China*

Correspondence should be addressed to Yiming Zhang; yiming.zhang@hebut.edu.cn

Received 27 January 2022; Revised 21 March 2022; Accepted 30 March 2022; Published 26 April 2022

Academic Editor: Yanan Gao

In situ fluidization mining is a promising method which shows considerable potential for reducing the ecological influence impacts of coal mining. During fluidization mining, coal gangue will be separated from the ores, filled back, and returned to the excavation region, which, depending on the filling rate, greatly reduces the stratum deformation of strata, depending on the filling rate. Numerical simulations can assist engineers in evaluating stratum deformation and optimizing affordable designs with affordable costs. Accordingly, in this work, a continuous–discontinuous element method is adopted, which is a coupled particle–block finite-discrete element method with an explicit integration formulation, which is adopted for simulating the coal in situ fluidization mining–filling processes. The theory concept of an "equivalent mining height" is utilized to define the backfill mining height. The results partly reveal the influences of the filling rate on the stratum deformation, surface subsidence, and rock burst phenomena, all of which further indicate the advantages of the fluidization mining method.

1. Introduction

With the increasing economic demand for coal resources, the long-term, high-intensity excavation of coal at shallow depths has exhausted the available coal resources near the surface; as a result, coal mining has gradually moved into deeper strata [1], while the mining scope of the current solid mineral mining method is relatively shallow [2, 3]. Traditional coal mining yields large volumes of waste known as gangue, the discharge of which can occupy land, pollute the environment, and endanger surface buildings. To reduce ecological damage, a novel method involving the in situ fluidization mining of deep coal [4] in which the coal gangue is separated from ores and placed back into the excavation region was proposed. Mining, selection and filling as one [5–9], backfill bodies, and coal pillars can help to control the settlement of strata and mitigate surface subsidence. Hence, these approaches can protect the environment while mining and converting deep coal in situ.

Field monitoring, theoretical analysis, and numerical simulation methods have been widely used to control surface subsidence, reduce ore pressures, and effectively reduce the impacts of waste on the surface. Zhou et al. [10] proposed the concept of the filling ratio and studied both the factors affecting the filling ratio. Sun [11] established a solid compaction and backfill mining dynamic model based on the key stratum theory for controlling rock layers, thereby providing a theoretical basis for determining the design of a solid backfill mining working face. Xu et al. [12] conducted numerical simulations to analyze the movement and deformation of the overburden in the stope and concluded that backfill mining can effectively control the failure degree of the overburden and reduce the stress concentration and influence range. Liu et al. [13] proposed a mechanical model of an elastic plate to analyze the coordinated instability of a coal pillar and roof and then specifically described an approach for evaluating the stability of the goaf and the design process for the filling parameters. With parameter studies, Zhao et al. [14] reported how the mechanical properties of the filling body affect the movement and stress of the roof. Feng et al. [15] proposed the concept of a backfill mining collaborative control system based on the specific

geological conditions of coal mines and analyzed the supporting characteristics of the overburden strata. Yu et al. [16] backfilled a mining roadway, established a mechanical model of roof settlement, and analyzed its control effects on ground settlement compared to traditional mining methods. Lu et al. [17] analyzed the stress distribution and deformation of backfill bodies through on-site ground monitoring and studied the boundary effect of backfill bodies. Zhao et al. [18] monitored the in situ stress and deformation of the working face and showed that the solid backfill technique could effectively reduce the failure degree of the overburden rock and control roof subsidence, thereby realizing the effective control of deformation in the overburden.

Considering complex geological environments, compared to experimental studies and on-site monitoring, numerical simulations can more economically identify the failure patterns and deformations of strata than can theoretical analyses. However, it is challenging for the conventional finite element method (FEM) to consider the cracking processes of strain-softening materials in a discrete manner. The increasing number of discontinuities affects the numerical stability and efficiency; as a result, in these types of cases, FEM models may not converge. Moreover, although some novel numerical methods, such as the cracking element method [19–24], cracking particle method [25–29], and peridynamics [30–34], can help to capture the initiation and propagation of fractures, in numerical simulations of fluidization mining, masses and gangue should be modeled by blocks and particles, respectively, which can fragment, requiring a numerical tool capable of handling the increased complexity of fragmented blocks and particles.

In this paper, the continuous-discontinuous element method (CDEM) coupled with the particle-block method (hereafter CDPB) is adopted for dynamically simulating the in situ replacement of coal in the goaf with gangue and studying the characteristics of the stope ore pressure and rock deformation. CDPB is a hybrid finite-discrete element method built in an explicit iterative numerical framework. The finite element procedure is used for small deformations of the system, and the discrete element procedure is used for large displacements and large deformations of the model. The concept of the "equivalent mining height" is used to define the in situ converted mining height of deep coal seams. By changing the filling ratio of gangue, surface subsidence can be controlled, which provides a theoretical basis for reducing the mine pressure and managing the resulting effects.

The remainder of this paper is organized as follows: the numerical method and constitutive model employed in this paper are presented in Section 2. Section 3 describes the simulation of in situ fluidization mining. In Section 4, the simulation results are presented and discussed. Finally, the concluding remarks are given in Section 5.

2. Numerical Method and Constitutive Model

2.1. Continuous-Discontinuous Element Method. The CDEM [35] is an explicit iterative numerical method that couples finite elements to discrete elements based on the Lagrange function, as shown in Equation (1). The numerical model is composed of block elements and interface elements: the block elements represent the continuous material characteristics, such as their elasticity/plasticity and damage, whereas the interface elements represent the discontinuous material characteristics, such as fracturing. Virtual springs are introduced between interface elements to transfer mechanical information, as shown in Figure 1. By setting the fracture criterion and mechanical parameters of these springs, the initiation, development, and propagation of multiple cracks can be simulated. Throughout the analysis, the force balance of the system is calculated by setting the unbalance rate:

$$\frac{d}{dt}\left(\frac{\partial L}{\partial \dot{u}_i}\right) - \frac{\partial L}{\partial u_i} = Q_i, \tag{1}$$

where Q_i is the nonconservative force of the system, L is the Lagrange function, u_i is the displacement of an element node, and $\dot{u}_i$ is the node velocity.

The control equation of CDEM is

$$\mathbf{M}\ddot{\mathbf{u}} + \mathbf{C}\dot{\mathbf{u}} + \mathbf{K}\mathbf{u} + \mathbf{K}_c\mathbf{u}_c + \mathbf{C}_c\dot{\mathbf{u}}_c = \mathbf{F}, \tag{2}$$

where $\ddot{\mathbf{u}}$, $\dot{\mathbf{u}}$, and $\mathbf{u}$ are the acceleration, velocity, and displacement matrices of the nodes of block elements. $\mathbf{u}_c$ and $\dot{\mathbf{u}}_c$ are the displacement and velocity matrices of the nodes of virtual interfaces. $\mathbf{M}$, $\mathbf{C}$, $\mathbf{K}$, $\mathbf{K}_c$, $\mathbf{C}_c$, and $\mathbf{F}$ are the unit mass, unit damping, unit stiffness, contact surface, contact surface damping, and node external load matrices, respectively. Based on the incremental method, the CDEM uses the explicit Euler predifference method to solve the problem. The unbalance degree of the system force is characterized by the unbalance rate. Equation (2) is solved in three steps: (i) calculating the deformation and damping forces of all elements, (ii) calculating the contact and damping forces of all interfaces, and (iii) calculating the external forces, accelerations, velocities, and displacements of all nodes.

2.2. Elastic Damage-Fracture Constitutive Model. In the numerical calculation, a linear elastic constitutive model is applied to the finite elements [36]. The resulting linear elastic constitutive model of finite elements is expressed by the incremental method:

$$\begin{cases} \Delta\sigma_{ij} = 2G\Delta\varepsilon_{ij} + \left(K - \dfrac{2}{3}G\right)\Delta\theta\,\delta_{ij}, \\ \sigma_{ij}(t_1) = \Delta\sigma_{ij} + \sigma_{ij}(t_0), \end{cases} \tag{3}$$

where σ_{ij} is the stress tensor, $\Delta\sigma_{ij}$ is the incremental stress tensor, $\Delta\varepsilon_{ij}$ is the incremental strain tensor, $\Delta\theta$ is the bulk strain increment, K is the bulk modulus, G is the shear modulus, t_1 is the next step, and t_0 is the current step.

The Mohr–Coulomb brittle fracture model is applied to the virtual interfaces to calculate the deformation and fracturing. The incremental method is used to calculate the

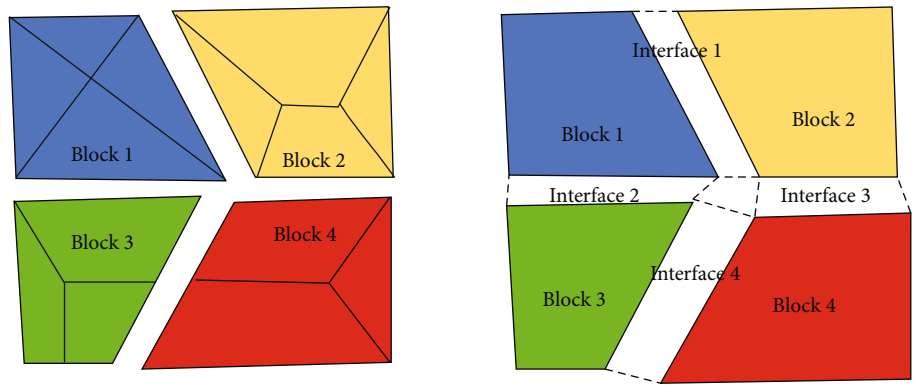

Figure 1: Block and interface elements of the CDEM.

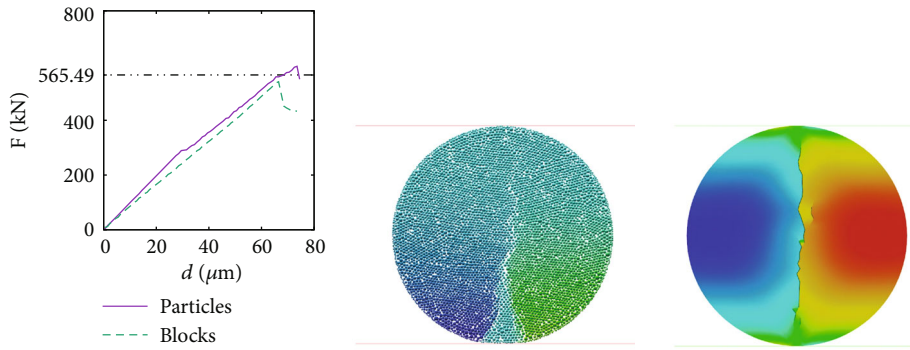

Figure 2: The results of the Brazilian disk test: (a) force-displacement curves; (b) failure patterns.

normal and tangential test contact forces in the next step on each virtual interface:

$$\begin{cases} F_n(t_1) = F_n(t_0) - K_n A_c \Delta du_n, \\ F_s(t_1) = F_n(t_0) - K_s A_c \Delta du_s, \end{cases} \tag{4}$$

where F_n and F_S are the normal and tangential contact forces, respectively; K_n and K_s are the normal and tangential contact stiffnesses, respectively, on the unit area (unit: Pa/m); A_s is the area of the virtual interface; and $\Delta d\, u_n$ and $\Delta d\, u_s$ are the normal and tangential relative displacement increments, respectively. Formula (5) and Formula (6) are used to judge tensile failure and correct the normal contact force and tensile strength.

If

$$-F_n(t_1) \geq \sigma_t(t_0) A_c, \tag{5}$$

then

$$\begin{cases} -F_n(t_1) = 0, \\ \sigma_t(t_1) = 0, \end{cases} \tag{6}$$

where $\sigma_t(t_1)$ is the tensile strength of the virtual interface at the next moment (unit: Pa). Formula (7) and Formula (8) are used to judge shear failure and correct the tangential contact force and cohesion.

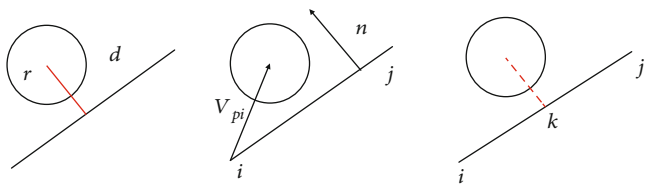

Figure 3: Point-edge contact model.

If

$$-F_s(t_1) \geq -F_n(t_1) \tan \phi + c(t_0) A_c, \tag{7}$$

then

$$\begin{cases} -F_s(t_1) = -F_n(t_1) \tan \phi + c(t_0) A_c, \\ c(t_1) = 0, \end{cases} \tag{8}$$

where ϕ is the internal friction angle of the virtual interface and $c(t_0)$ and $c(t_1)$ are the cohesion of the virtual interface at the initial moment and the next moment, respectively (unit: Pa).

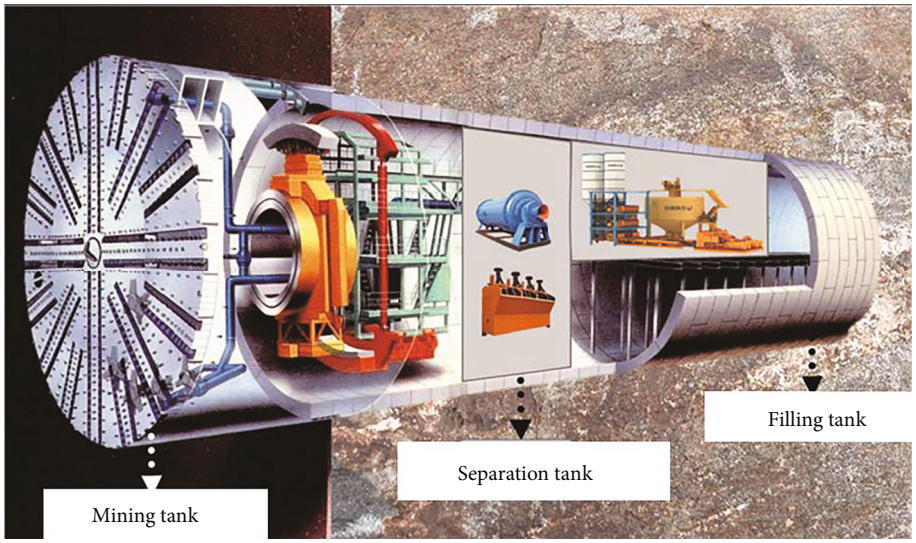

Figure 4: In situ fluidization mining process [39].

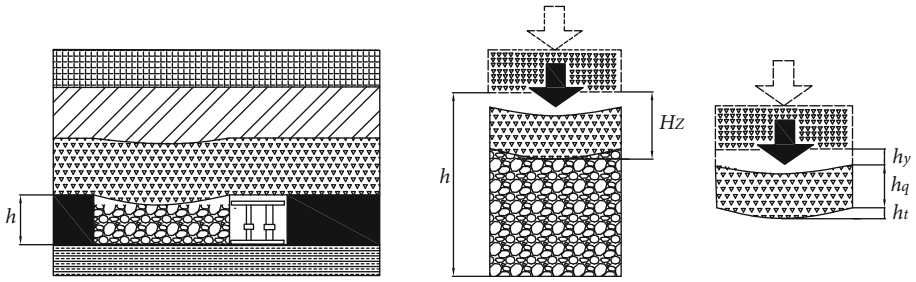

Figure 5: Equivalent mining height model of solid backfilling.

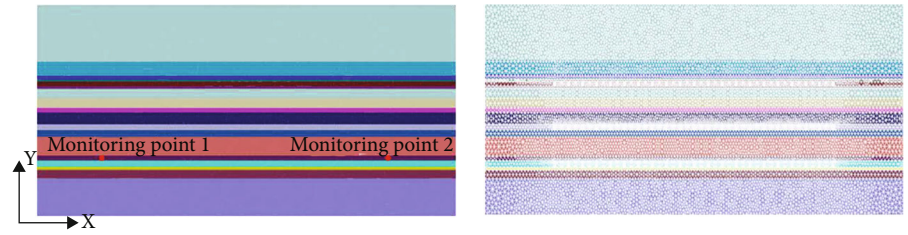

(a) (b)

Figure 6: Model overview: (a) numerical model; (b) mesh.

2.3. Validation. The Brazilian disk test is used to validate the numerical tool. We used the same setup provided in [37], where the diameter D and tensile strength f_t of the disk are taken as 6 cm and 6 MPa, respectively. The disk is built with particles and blocks. The peak load per unit thickness F can be determined by

$$F = \frac{\pi D f_t}{2} = 565.49\,\text{kN}. \tag{9}$$

The obtained force-displacement curves and failure patterns are shown in Figure 2. The peak load is generally close to the analytical solution, and the failure pattern is also agreeable.

2.4. Coupled Particle-Block System. This work considers the coupling of block and particle discrete elements [38]. The coupling processes include (i) detecting the particle-block contact and (ii) calculating the contact force. The contact force is obtained by the incremental method:

$$\begin{cases} F_n(t+\Delta t) = F_n(t) - K_n \Delta du_n, \\ F_s(t+\Delta t) = F_s(t_0) - K_s \Delta du_s, \end{cases} \tag{10}$$

Table 1: Rock material parameters.

Lithology	Roof depths (m)	Bulk modulus (GPa)	Shear modulus (GPa)	Density (kg/m^3)	Cohesion (MPa)	Tensile strength (MPa)	Friction angle (°)
Medium sandstone	730	3.31	1.71	2650	18.5	11.2	41
Sandy mudstone	737.4	1.6	0.9	2610	9.5	7.5	36
Medium sandstone	739.4	3.31	1.7	2650	18.5	11.2	41
Mudstone	740.7	1.82	0.91	2630	9	4.4	38
No. 5 coal	742.9	1.14	0.45	1340	3	12	26
Siltstone	744.3	4.35	2	2710	13	10	44
Fine sandstone	749.5	3.31	1.71	2700	18.5	12	41
Mudstone	754.5	1.82	0.91	2620	9	10	38
Siltstone	756.9	3.69	1.61	2650	18	12.5	45
Sandy mudstone	763.2	1.87	0.87	2300	12	11	36
No. 8 coal	766.2	0.73	0.3	1310	2.8	1	28
Mudstone	769.8	0.94	0.36	2300	4	3	36
Siltstone	779.8	3.5	1.53	2650	18	12.5	45
Mudstone	783.2	0.94	0.36	2300	4	3	36
No. 9 coal	785.8	1.14	0.45	1310	2.8	1.4	28
Sandy mudstone	787.3	1.87	0.87	2300	12	11	36
Mudstone	791.8	0.94	0.36	2300	3	3	36
Siltstone	811	2.955	2.18	2650	18	12.5	45

Table 2: Gangue material parameters.

Lithology	Filling ratio	Density (kg/m^3)	Cohesion (MPa)	Tension (MPa)	Friction angle (°)
Gangue filling body	70%/80%/90%	1200	0.3	0.1	10

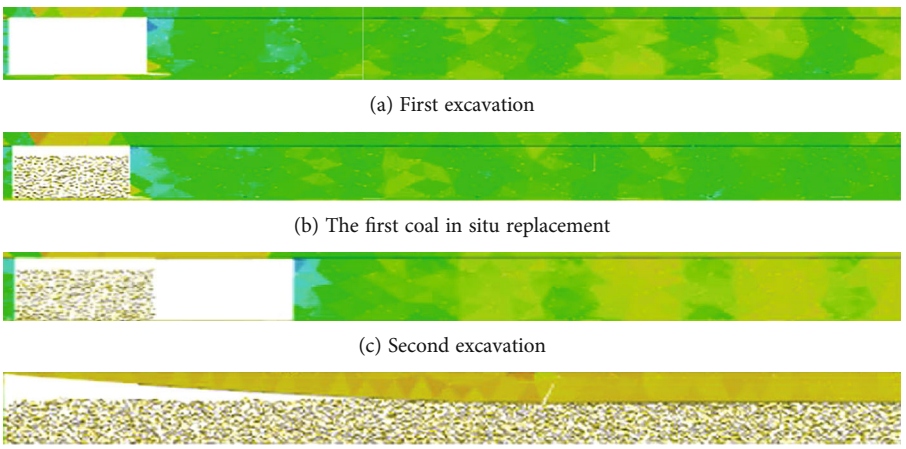

(a) First excavation

(b) The first coal in situ replacement

(c) Second excavation

(d) All coal in situ replacement

Figure 7: Coal seam mining and in situ conversion.

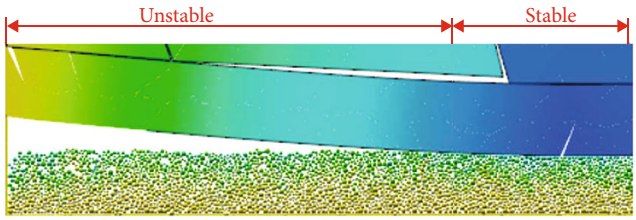

Figure 8: Collaborative support mechanism.

where $\Delta d u_n$ and $\Delta d u_s$ represent the normal and tangential displacement differences (cracking openings), respectively, between the contact particles.

The formula for calculating the contact torque is as follows:

$$\begin{cases} M_n(t+\Delta t) = M_n(t) - \dfrac{K_s J \Delta d u_n}{A_c}, \\ M_s(t+\Delta t) = M_s(t) - \dfrac{K_n I \Delta d u_s}{A_c}, \end{cases} \tag{11}$$

where M_n and M_s are the torque and bending moment, respectively; I and J are the moment of inertia and polar moment of inertia of the contact surface, respectively; and $\Delta d u_n$ and $\Delta d u_s$ are the incremental differences in the torsion and bending angle between particles, respectively.

Particle-block contacts are detected in two steps: preliminary detection and accurate detection. The preliminary detection step is achieved by the subspace method. The scope of retrieval can be reduced by the mapping relationship among particles, cells, and grid areas. The accurate detection step locates the contact between a particle and the boundary of the finite element. The point-edge contact model is adopted, as shown in Figure 3. The creation of a point-edge contact should satisfy two conditions simultaneously: first, the distance d from the particle centroid to the boundary edge d (as shown in Equation (12)) must be less than or equal to the particle radius r; second, the projected location of the particle centroid on the boundary edge is located inside the edge $(d_{ik} \le d_{ij}, d_{jk} \le d_{ij})$, where V_{pi} is the relative position vector from i to particle p and n is the outer normal vector of the edge. Once the particle is in contact with an edge, normal and tangential springs are automatically created. The interpolation coefficient of the contact point k is solved by Equation (13):

$$d = \left| V_{pi} \bullet n \right|, \tag{12}$$

$$\begin{cases} w_i = \dfrac{d_{jk}}{d_{ij}}, \\ w_j = \dfrac{d_{ik}}{d_{ij}}. \end{cases} \tag{13}$$

2.5. In Situ Fluidization Mining. In conventional mining, coal mining and production processes are independent. The coal and coal gangue (solid waste) will be transported together to the surface through a pipeline. Then, a "gangue mountain" will be formed on the surface before backfill, potentially causing pollution. In addition, the costs of transportation and backfill will increase dramatically for deep mining. In situ fluidization mining is a method combining the mining and production processes that separates coal and gangue in situ as an economical and eco-friendly mining method. Moreover, compared to conventional caving mining, since gangue is backfilled in site, fluidization mining can reduce the stratum deformations and mitigate the fracturing of the roof.

In situ fluidization mining includes mining, separation, and filling processes (see Figure 4). In the process of unattended mining, an underground tunnel drilling machine is used for mining treatment. The minerals are separated and sorted in the separation tank. Under the action of gravity, the slag mixture is selected to form the backfill material, which is backfilled to the excavated area. In the next sections, considering the equivalent mining height theory, the surface subsidence and ore pressures of fluidization mining will be studied and compared to conventional mining methods.

2.6. Equivalent Mining Height Theory. In the process of filling the mining face with gangue, the coal is converted in situ. While the coal to be mined remains in front of the working face, solid waste materials such as gangue are filled into the goaf, occupying parts of the stope. The actual coal seam thickness is reduced. This process can be regarded as extremely thin coal seam mining. The equivalent mining height [40] H_z depends on the roof displacement and filling body compression. As shown in Figure 5. The maximum excavation height is the equivalent mining height after backfill mining. Furthermore, the deformation of the overlying strata, surface subsidence, and ore pressure of in situ fluidization mining depend on the filling ratio of gangue.

The equivalent mining height H_z of gangue filling is

$$H_z = h_t + h_q + h_y, \tag{14}$$

where h_t is the amount of roof subsidence known in advance, h_q is the amount of nonconnection, and h_y is the amount of compressed filling body, which can be obtained by

$$h_y = \eta\left(h - h_t - h_q\right), \tag{15}$$

where h is the total mining height after backfill mining (m), and η is the compression ratio of the filling body. η depends on the porosity:

$$\eta = k_0 - k_n, \tag{16}$$

where k_0 and k_n are the porosities of the filling solid after initial and final compaction, respectively. Hence, H_z is

$$H_z = h_t + h_q + \eta\left(h - h_t - h_q\right). \tag{17}$$

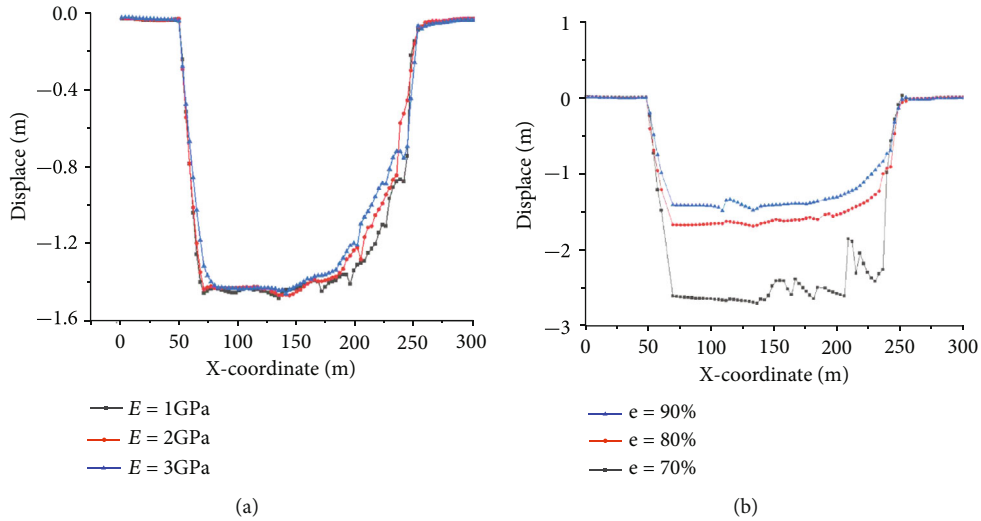

Figure 9: Long-term roof subsidence: (a) long-term roof subsidence for filling materials with different elastic moduli; (b) long-term roof subsidence for filling materials with different filling rates.

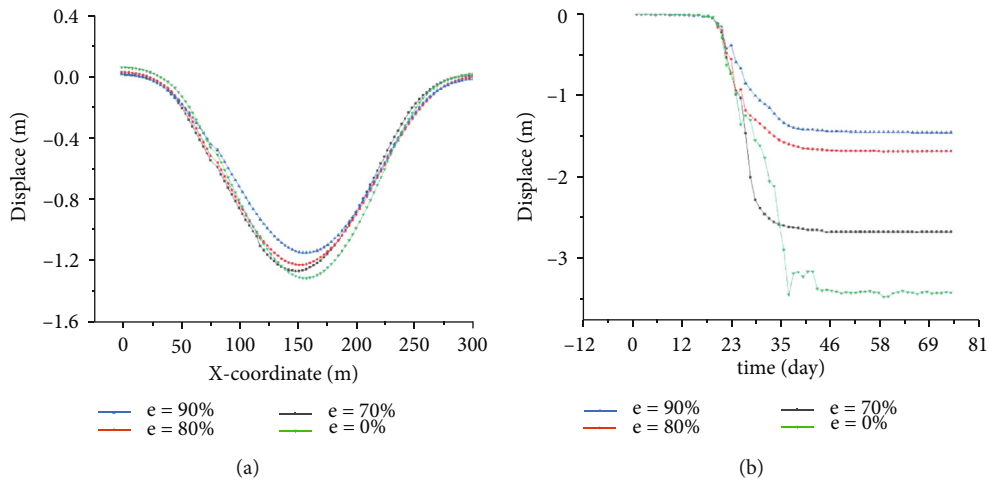

Figure 10: Subsidence curves: (a) ground subsidence curve; (b) roof subsidence curve.

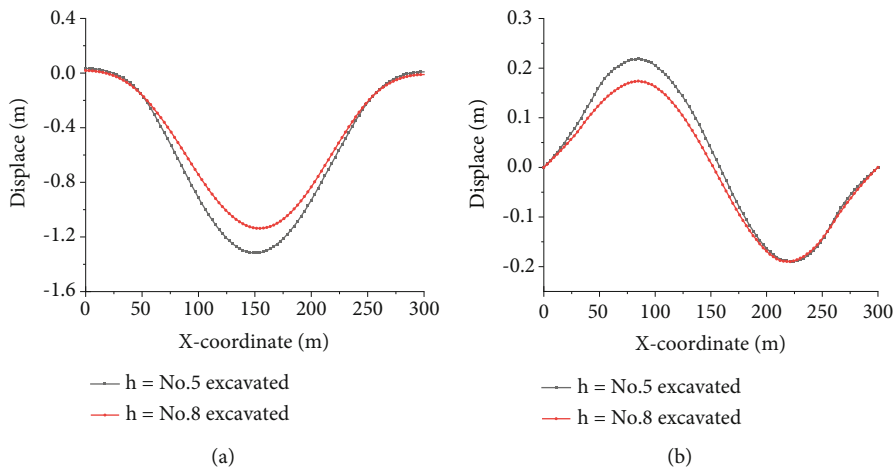

Figure 11: Ground deformation curves: (a) ground vertical displacement; (b) ground horizontal displacement.

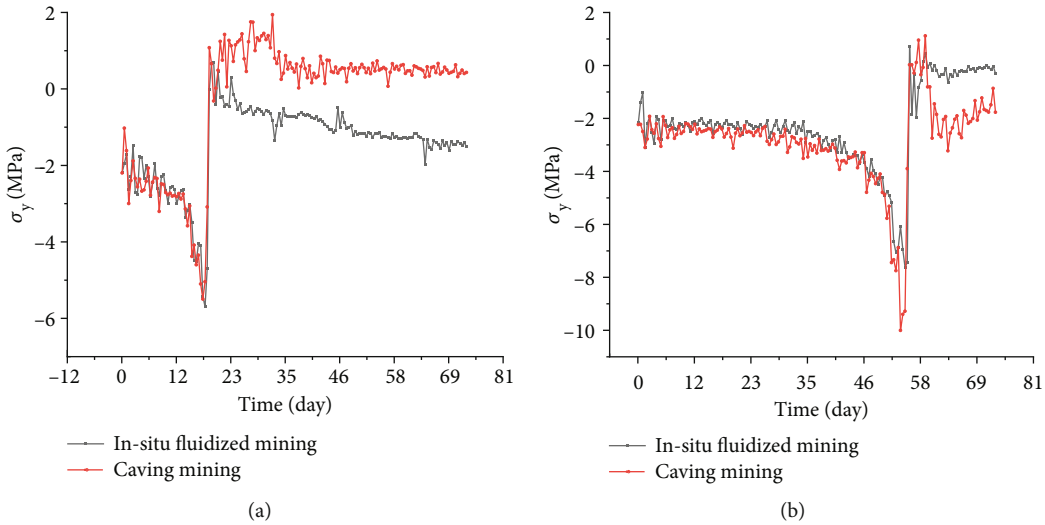

Figure 12: Evolution of the vertical stress component σ_y: (a) monitoring point 1; (b) monitoring point 2.

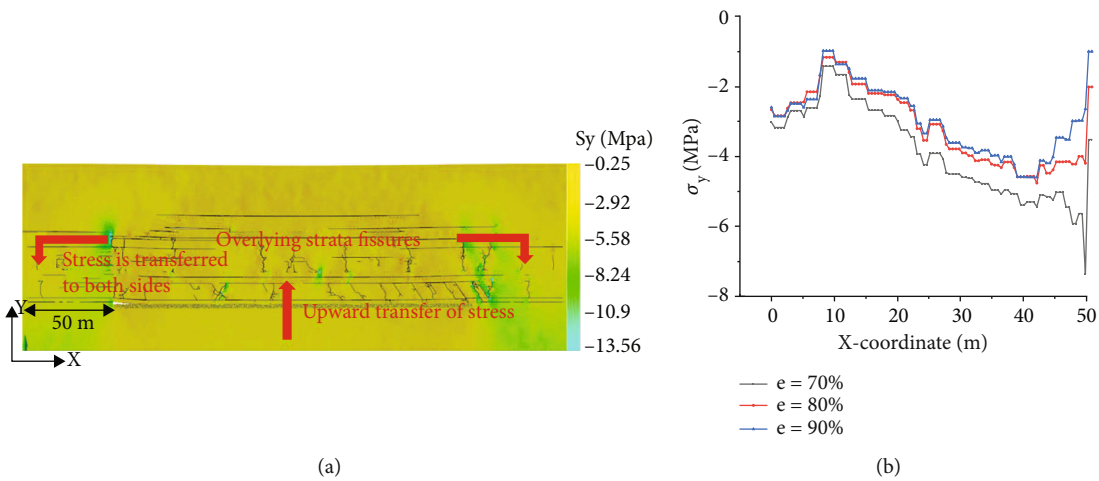

Figure 13: The distributions of σ_y of in situ fluidization mining: (a) the contour plot of σ_y considering a filling ratio of 90%; (b) the distributions of σ_y of coal pillar considering different filling ratios.

3. Numerical Simulation of the In Situ Conversion and Mining of Deep Coal Resources

3.1. Engineering Background. The Kailuan Group Tangshan mining area is located in Tangshan, Hebei Province. Within this area, coal seams 5, 8, and 9 are thick, stable, and recoverable. These coal seams are located at depths of 700 ~ 800 m and thus are considered deep coal seams. The in situ converted goaf is located in the No. 9 coal seam, and the thickness of the coal seam is 3.5 m. The ore pressures are imposed by the buildings, railways, and water bodies at the surface above the mine field, approximately 171 million tons. With the conventional mining method, 800,000 tons of coal gangue is discharged annually to the surface, occupying a great amount of land.

Based on the working face in the above coal seam, considering the height of each layer and boundary effects, the numerical model established in this study is 300 m long and 111 m high. The model and mesh of the example are shown in Figure 6. Two measuring points are prescribed in the model at a distance of 1.5 m below the roof and 100 m from the left and right boundaries of the coal seam. The material parameters of the mining strata are shown in Table 1, where the interface parameters are set according to stratum parameters, including stiffness parameters and strength parameters. The stiffness is 10 times that of the rock layer, and the strength is 3 times that of the rock layer. Gmsh software is used to discretize the model into 13,849 nodes and 27,255 elements, assuring the accuracy and efficiency.

3.2. Simulation Process. The numerical simulation includes three stages. The first stage is the elastic stage, in which boundary normal constraints are applied to the left and right sides and the bottom of the material. Then, the in situ stress exerted by the overlying strata is initialized at the top of the model. The block element and interfaces are both linear elastic materials. In the second stage, the material model adopts

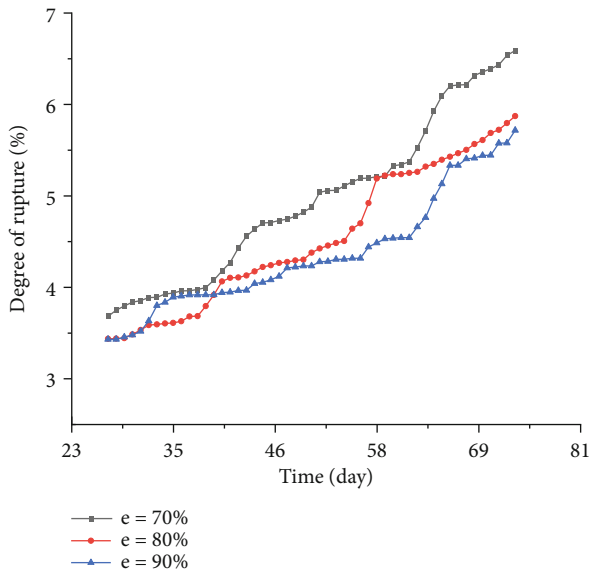

Figure 14: Long-term rupture degree considering different filling ratios.

the Mohr–Coulomb model, whereas the virtual interfaces adopt the brittle fracture model. In this elastic-plastic stage, the static stress field under the influence of gravity is solved by using the virtual mass method, and the stress balance is obtained. The third stage is the coal seam mining and gangue filling stage, considering the coupled particle-block contact effects. The goaf is created by excavating the coal seam from left to right at an interval of 5 m for 40 iterations. In the next section, if it is not specified, the No. 9 coal seam will be mined. The coal gangue is filled into the goaf after each excavation to replace part of the stope. Therefore, coal pillars and the gangue filling body support the overlying strata and help to reduce ground subsidence and mitigate rockburst. In the numerical studies, we also consider different filling ratios of coal gangue and compare fluidization mining to conventional caving mining. The gangue parameters are shown in Table 2. After excavating the working face, the coal pillars in certain sections are set as empty models, and then, the goaf is backfilled with coal gangue particles with different filling ratios, supporting the overlying strata, as shown in Figure 7.

4. Results and Discussion

4.1. Deformation of the Roof. The strata overlying the backfill exhibit compression deformation in the long term. However, because of the frictional forces among the gangue particles inside the filled goaf, the grain-scale deformation of the filling body gradually becomes stable. Initially, there is no supporting effect on the roof, and the roof exerts no pressure on the gangue filling body in the beginning. When the roof subsides to the equivalent mining height, part of the roof is supported by the filling body and coal pillar, and some pores among the particles in the gangue filling body are compressed, restricting the settlement of the roof, as illustrated in Figure 8.

The supporting performance of different filling materials depends on (i) the deformation moduli of the backfill material and (ii) the filling ratio. Considering different elastic moduli of the backfill material and filling ratios, the long-term roof subsidence is illustrated in Figure 9.

According to Figure 9, the elastic moduli of the filling materials have relatively small influences on the roof subsidence, while the filling ratios have much greater influences. In each curve, there is a platform part at the bottom where the coal gangue filling material has reached the maximum compression and the equivalent mining height has reached.

4.2. Ground Subsidence. The ground subsidence depends on the filling ratio and mining depth. The filling ratios of 0%, 70%, 80%, and 90% are considered for investigating their influences on ground subsidence, in which a 0% filling ratio is close to that of traditional caving mining. The long-term ground subsidence is shown in Figure 10(a), indicating that higher filling ratios help to control the ground subsidence. Considering monitoring point 1 (see Figure 6), the evolution of its displacement is shown in Figure 10(b). Figure 10(b) shows that the stabilization of the roof for all filling ratios will take more than 10 days. Moreover, for the case with a filling ratio of 0%, the displacement curve is not very smooth, mainly caused by serious fragmentation of the bent roof.

To investigate the influence of excavation depth on ground subsidence, excavations of coal seams No. 5 and No. 8 in Table 1 are considered. The ground deformation (vertical and horizontal displacement) curves are shown in Figure 11. The results indicate that the ground displacements decrease with increasing mining depth.

4.3. Deformation and Failure Pattern of the Coal Seam. Considering a filling ratio of 90%, the evolutions of the vertical stress component σ_y at monitoring points 1 and 2 (see Figure 6) are shown in Figure 12. The results indicate that at both points, the peak stresses of fluidization mining are smaller than those of caving mining, which helps to reduce rockburst events.

Considering a filling ratio of 90%, the contour plot of σ_y is shown in Figure 13(a), indicating that the roof breaks like a deep beam under self-weight. For different filling ratios, the distributions of σ_y of the coal pillar are shown in Figure 13(b), indicating that the supporting stress decreases with increasing filling ratio.

The rupture degree is defined as the ratio of the area of activated interface elements to the area of all interface elements implemented in numerical calculations. For different filling ratios, the evolution of the rupture degree is shown in Figure 14. The rupture degree decreases with increasing filling rate.

5. Conclusion

Coupled particle-block elements built in the framework of CDEM are used for simulating the in situ fluidization mining processes of a deep coal seam where the coal gangue is filled back. The responses of the strata are analyzed and

compared to those of traditional caving mining. Some conclusions are drawn: (i) to control the roof and ground subsidence, the filling ratio of coal gangue has a greater influence than its mechanical properties. When the filling rate increases from 70% to 90%, the roof settlement decreases by 1 m, and the ground subsidence decreases by 0.12 m. (ii) In situ fluidization mining greatly helps to control the fragmentation and deformation of strata. When the filling rate increases from 70% to 90%, the peak stress decreases by 2.5 MPa, and the rupture degree decreases by 1%.

Data Availability

The data used to support the findings of this study are included within the article.

Conflicts of Interest

The authors declare that they have no conflicts of interest.

Acknowledgments

The authors gratefully acknowledge the financial support from the National Natural Science Foundation of China (NSFC) (52178324) and National Key Research and Development Project of China, The Ministry of Science and Technology of China (2018YFC1505504).

References

[1] J. Du, J. Chen, Y. Pu, D. Jiang, L. Chen, and Y. Zhang, "Risk assessment of dynamic disasters in deep coal mines based on multi-source, multi-parameter indexes, and engineering application," *Process Safety and Environmental Protection*, vol. 155, pp. 575–586, 2021.

[2] H. P. Xie, F. Gao, Y. Ju et al., "Quantitative definition and investigation of deep mining," *Journal of coal*, vol. 37, no. 4, p. 8, 2012.

[3] H. P. Xie, F. Gao, Y. Ju et al., "Basic theory and engineering practice of deep mining," *Journal of coal*, vol. 40, no. 1, p. 10, 2015.

[4] H. P. Xie, F. Gao, Y. Ju, M. Z. Gao, and R. Zhang, "Groundbreaking theoretical and technical conceptualization of fluidized mining of deep underground solid mineral resources," *Tunnelling and Underground Space Technology*, vol. 67, pp. 68–70, 2017.

[5] S. Sriramoju, D. Kumar, S. Majumdar, P. Dash, D. Shee, and R. Banerjee, "Sustainability of coal mines: separation of clean coal from the fine-coal rejects by ultra-fine grinding and density-gradient-centrifugation," *Powder Technology*, vol. 383, pp. 356–370, 2021.

[6] H. Zhang, Q. Zhang, X. Zuo et al., "Design and application of ecological environment protection mining, dressing and filling system," *Journal of China University of Mining and Technology*, vol. 50, no. 3, p. 10, 2021.

[7] S. H. Tu, Y. Hao, D. K. Miao, X. Liu, and W. L. Li, "Deep mining, beneficiation and filling integrated complex mine system cooperative mining," *Journal of China University of Mining and Technology*, vol. 50, no. 3, p. 11, 2021.

[8] S. H. Tu, D. Y. Hao, W. L. Li et al., ""Construction of mining, beneficiation and filling +x" integrated selective mining theory and technology system," *Journal of Mining and Safety Engineering*, vol. 37, no. 1, p. 12, 2020.

[9] J. X. Zhang, Q. Zhang, F. Ju, N. Zhou, M. Li, and W. Q. Zhang, "Technical system and engineering practice of "mining, beneficiation and filling +x" green mining in coal mine," *Journal of coal*, vol. 44, no. 1, p. 10, 2019.

[10] Y. J. Zhou, Y. Chen, J. X. Zhang, and Q. He, "Control principle and technology of final compression ratio of backfilling materials," *Caikuang yu Anquan Gongcheng Xuebao/Journal of Mining and Safety Engineering*, vol. 29, no. 3, pp. 351–356, 2012.

[11] J. Sun, "Mechanics criterion and factors affecting overburden stability in solid dense filling mining," *Mining Science and Technology*, vol. 27, no. 3, pp. 407–413, 2017.

[12] Y. Xu, Q. Chang, H. Zhou, Z. Cao, X. Li, and J. Chen, "Movement and deformation laws of the overlying strata in paste filling stope," *Mining Science and Technology (China)*, vol. 21, no. 6, pp. 863–868, 2011.

[13] C. Liu, Z. Tan, K. Deng, and P. Li, "Synergistic instability of coal pillar and roof system and filling method based on plate model," *Mining Science and Technology*, vol. 23, no. 1, pp. 145–149, 2013.

[14] X. Y. Zhao, X. W. Li, K. Yang, Z. Wei, and Q. Fu, "The segmental subsidence structure with immediate roof of gob side entry retaining in backfill mining," *Energy Exploration & Exploitation*, no. 4, article 014459872199654, 2021.

[15] J. U. Feng, C. Zhiwei, Z. Qiang, H. Peng, T. Yang, and L. Lixin, "Surrounding rock stability control in gob-side entry retaining with solid backfilling in coal mining technology," *Journal of Mining & Safety Engineering*, vol. 32, no. 6, p. 936, 2015.

[16] Y. Yu, L. Ma, and D. Zhang, "Characteristics of roof ground subsidence while applying a continuous excavation continuous backfill method in longwall mining," *Energies*, vol. 13, 2020.

[17] R. Lu, F. Ma, J. Zhao, J. Wang, G. Li, and B. Dai, "Monitoring and analysis of stress and deformation features of boundary part of backfill in metal mine," *Sustainability*, vol. 12, no. 2, p. 733, 2020.

[18] T. B. Zhao, Z. Y. Fu, and L. Gang, "In situ investigation into fracture and subsidence of overburden strata for solid backfill mining," *Arabian Journal of Geosciences*, vol. 11, no. 14, p. 398, 2018.

[19] Y. Zhang, R. Lackner, M. Zeiml, and H. Mang, "Strong discontinuity embedded approach with standard SOS formulation: element formulation, energy-based crack-tracking strategy, and validations," *Computer Methods in Applied Mechanics and Engineering*, vol. 287, pp. 335–366, 2015.

[20] Y. Zhang and X. Zhuang, "Cracking elements: a self-propagating strong discontinuity embedded approach for quasi-brittle fracture," *Finite Elements in Analysis and Design*, vol. 144, pp. 84–100, 2018.

[21] Y. Zhang and X. Zhuang, "Cracking elements method for dynamic brittle fracture," *Theoretical and Applied Fracture Mechanics*, vol. 102, pp. 1–9, 2019.

[22] Z. Sun, X. Zhuang, and Y. Zhang, "Cracking elements method for simulating complex crack growth," *Journal of Applied and Computational Mechanics*, vol. 5, no. 3, pp. 552–562, 2018.

[23] L. Mu and Y. Zhang, "Cracking elements method with 6-node triangular element," *Finite Elements in Analysis and Design*, vol. 177, article 103421, 2020.

[24] Y. Zhang, J. Huang, Y. Yuan, and H. A. Mang, "Cracking elements method with a dissipation-based arc-length approach," *Finite Elements in Analysis and Design*, vol. 195, article 103573, 2021.

[25] T. Rabczuk and T. Belytschko, "Cracking particles: a simplified meshfree method for arbitrary evolving cracks," *International Journal for Numerical Methods in Engineering*, vol. 61, no. 13, pp. 2316–2343, 2004.

[26] T. Rabczuk and T. Belytschko, "Adaptivity for structured meshfree particle methods in 2D and 3D," *International Journal for Numerical Methods in Engineering*, vol. 63, no. 11, pp. 1559–1582, 2005.

[27] T. Rabczuk and G. Zi, "A meshfree method based on the local partition of unity for cohesive cracks," *Computational Mechanics*, vol. 39, no. 6, pp. 743–760, 2007.

[28] T. Rabczuk, S. Bordas, and G. Zi, "A three-dimensional meshfree method for continuous multiple-crack initiation, propagation and junction in statics and dynamics," *Computational Mechanics*, vol. 40, no. 3, pp. 473–495, 2007.

[29] T. Rabczuk and T. Belytschko, "A three-dimensional large deformation meshfree method for arbitrary evolving cracks," *Computer Methods in Applied Mechanics and Engineering*, vol. 196, no. 29-30, pp. 2777–2799, 2007.

[30] H. Ren, X. Zhuang, Y. Cai, and T. Rabczuk, "Dual-horizon peridynamics," *International Journal for Numerical Methods in Engineering*, vol. 108, no. 12, pp. 1451–1476, 2016.

[31] H. Ren, X. Zhuang, and T. Rabczuk, "Dual-horizon peridynamics: a stable solution to varying horizons," *Computer Methods in Applied Mechanics and Engineering*, vol. 318, pp. 762–782, 2017.

[32] H. Yu, X. Chen, and Y. Sun, "A generalized bond-based peridynamic model for quasi-brittle materials enriched with bond tension-rotation-shear coupling effects," *Computer Methods in Applied Mechanics and Engineering*, vol. 372, article 113405, 2020.

[33] H. Yu and Y. Sun, "Bridging the gap between local and nonlocal numerical methods–a unified variational framework for non-ordinary state-based peridynamics," *Computer Methods in Applied Mechanics and Engineering*, vol. 384, article 113962, 2021.

[34] Y. Zhang, X. Yang, X. Wang, and X. Zhuang, "A micropolar peridynamic model with non-uniform horizon for static damage of solids considering different nonlocal enhancements," *Theoretical and Applied Fracture Mechanics*, vol. 113, article 102930, 2021.

[35] F. E. Chun, L. I. Shihai, Z. H. Bingxu, C. U. Xiaorong, and J. I. Jianjun, "Numerical simulation on complete process of three-dimensional bench blasting in open pit mine based on cdem," *Explosion and Impact*, vol. 39, no. 2, p. 11, 2019.

[36] C. Feng, S. Li, and J. Wang, "Sability analysis method of bedding rock slopes under seismic load based on cdem," *Journal of Geotechnical Engineering*, vol. 34, no. 4, pp. 717–724, 2012.

[37] Y. Zhang and H. A. Mang, "Global cracking elements: a novel tool for galerkin-based approaches simulating quasi-brittle fracture," *International Journal for Numerical Methods in Engineering*, vol. 121, no. 11, pp. 2462–2480, 2020.

[38] E. Onate and J. Rojek, "Combination of discrete element and finite element methods for dynamic analysis of geomechanics problems," *Computer Methods in Applied Mechanics and Engineering*, vol. 193, no. 27-29, pp. 3087–3128, 2004.

[39] H. P. Xie, F. Gao, Y. Ju et al., "Theoretical and technological conception of the uidization mining for deep coal resources," *Journal of China Coal Society*, vol. 42, no. 3, pp. 547–556, 2017.

[40] X. Miu, Y. Huang, F. Ju, X. Mao, G. L. Guo, and J. Zhang, "Strata movement theory of dense backfill mining," *Journal of China University of Mining and Technology*, vol. 41, no. 6, p. 5, 2012.